CORPUS PUBLISHERS

Journal of Mineral and Material Science (JMMS)

Volume 3 Issue 2, 2022

Article Information

Received date :June 19, 2022

Published date: June 27 2022

*Corresponding author

Alghamdi SK, Department of Physics, Faculty of Science, Taibah University, Al-Madina al Munawarah, Saudi Arabia

Keywords

UV spectroscopy; XRD; Makrofol; Plasma

Abbreviations

VLG 7-1: Makrofol; XRD: X-Ray Diffraction; UVs: Ultraviolet Spectroscopy; NTD: Nuclear Track Detector; Hz: Hertz

Research Article

Effect of Plasma Exposure on the Structural and Optical Properties of Makrofol VLG 7-1 Nuclear Track Detector

Alghamdi SK*

Department of Physics, Faculty of Science, Taibah University, Al-Madina al Munawarah, Saudi Arabia

Abstract

Makrofol VLG 7-1 is a sort of Makrofol (bisphenol-A polycarbonate) nuclear track detector. We believe that the current study is the first one that deals with the effect of plasma irradiation on Makrofol VLG 7-1. Samples of Makrofol films were treated with various plasma exposure times (300-1800 sec.) The resultant outcome of the plasma irradiation on the structure and optical characteristics of the Makrofol samples were explored applying X-Ray Diffraction (XRD) and Ultraviolet Spectroscopy (UVs). The optical band gap, refractive index, and optical dielectric parameters were characterized and interpreted based on the exposure time. The optical bandgap decreased with increasing the exposure time up to 1800 sec. We attribute this to the dominance of crosslinking that damaged the crystalline portion.

Introduction

Makrofol (bisphenol-A polycarbonate) is a type of amorphous Nuclear Track Detector (NTD). It's a thermoplastic polymer that stands out for its outstanding optical properties [1]. It's also a good choice for medicinal and dosimeter applications [2-4]. Makrofol is a type of NTDs whose characteristics vary based on the conditions of manufacture. As a result, when subjected to ionizing radiations, its reactions will vary [1]. Makrofol VLG 7-1is developed for applications requiring thermoforming. Makrofol contains carbonyl groups, which are radiation-sensitive group. It degrades more quickly than the phenyl group under the influence of low radiation doses, and so is responsible for Makrofol damage caused by radiation [5]. Makrofol's low density and exceptional transparency make it suitable for optical fibers and electronic devices. These distinguishing features also make it a viable choice for use in dosimetry. It is widely utilized in alpha, neutron, and charged particle radiography, track-etched membrane preparation, radiation dosimetry, and cosmic ray detection, also for low linear energy transfer radiation like UV radiation and gamma rays [6,7]. Despite Makrofol has a high commercial and technical presentation, structural deficiencies in Makrofol samples are caused by uncontrollable factors such as humidity and temperature change during the polymerization process. This results in structural deficiencies, as well as alterations in its physical characteristics and poor thermostability. Radiation processing can help to decrease the generated structural deficiencies. During the bond cleavage of the chains, radiation produces active catalytic free radicals that contribute in the creation of new bonds, generating crosslinks. As a result, the macromolecular structure of Makrofol is affected, as is its shape. This occurs without changing the molecular structure of the substance [8]. Furthermore, the impact of radiations causes lattice defects, which alter the characteristics of the polymer [9,10].

Characterizing the optical properties of polymers is very important because of their widespread use in optoelectronic devices [11,12]. The refractive index of polymers provides information on their fundamental properties [11]. Furthermore, the change in refractive index with radiation dose contributes in the evaluation of the polymer's optical behavior. This is critical information for them to be used in industry [12], as it is applicable to marketable applications such as radiation dosimetry and processing [13]. Several researchers have investigated the structural and optical changes in irradiated polymers for dosimeter purposes [14-16]. The ensuing free radicals, benzophenones, re-arranged isopropylidene radicals, and creation of stronger conjugated bonds are responsible for the change in optical characteristics of Makrofol caused by irradiation [17]. The main goal of this research was to obtain information concerning the interaction of plasma with Makrofol aiming to improve its structural and optical properties and refining its performance in a variety of applications.

Experiment

Samples

Farbenfabriken Bayer A.G. (Germany) produced Makrofol VLG 7-1 films with a thickness of 380 μm and a density of 1.2 g/cm^3 density. They had a higher light transmission rate (90.3 percent). $C_{16}H_{14}O_3$ is the chemical formula. Makrofol VLG 7-1 is a high-pressure forming and thermoforming material.

Exposure facility

The plasma-generating chamber was cylindrical in design, with a diameter of 25 cm and a height of 36 cm. It is composed of stainless steel. It consisted of two stainless-steel electrode plates, each with a diameter of 5 cm and a space of 2.5 cm between them. An RF power supply and an impedance matching network were used to connect the two electrodes, which were positioned inside dielectric ceramics. An RF source (type ENI model OEM-6, 13.56 MHz, 0–200 W power) was used to power the lower electrodes, while the upper anode was grounded. The chamber was brought to a base pressure of 10-4 torr using a rotary pump. The air gas pressure was set at 1.0 torr and remained constant during the measurements.

Analyzation of the exposed samples

The X-ray diffraction was measured using a Shimadzu 6000 diffractometer, which is noted for its Cu-k radiation. The X-rays had a wave length of 1.54 Å and the diffraction patterns were taken in the 2q at a rate of 2° per minute, ranging from 10° to 60°. The Tomos UV-1800 Spectrophotometer was used to measure UV spectra at wavelengths ranging from 800 to 200 nm.

Results and Discussion

XRD analysis

The change in the ratio of ordered to disordered regions due to plasma exposure was investigated using X-ray diffraction. Figure 1 shows the XRD curves for the exposed and non-exposed Makrofol films for samples recorded within 2q (10-60 degrees). The results' analysis indicates a disordered halos (2q=12-23°) implying disordered regions' dominance. As can be seen, integral intensity, or the area under the curve, decreases as exposure duration increases up to 1800 seconds. As a consequence of crosslinking, which decreases crystallinity, the disorder nature of the samples increases. Crosslinking causes the integral intensity to decrease, resulting in the breakdown of ordered structure. This reduction shows that plasma exposure causes regular lamellas to crosslink, resulting in non-arranged lamellas.

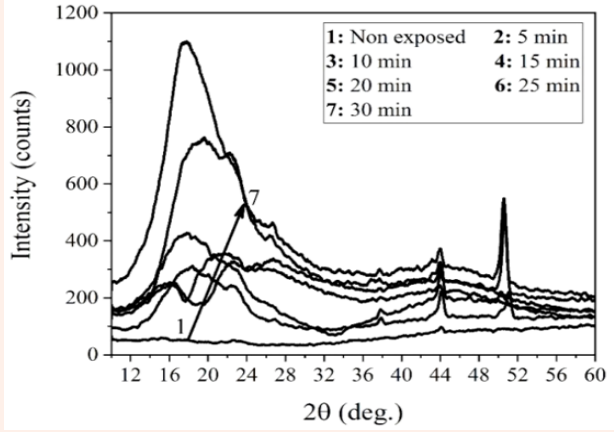

Figure 1: XRD spectra of the exposed and non-exposed Makrofol films.

Optical analysis of plasma exposed Makrofol films

Absorption: Figure 2 shows the absorbance of UV spectra of exposed and non-exposed Makrofol films in order to compute band-gap configuration changes owing to plasma exposure and get insight into optically induced electronic transitions. At about 250 nm, a prominent absorption band was discovered, which was minimized when the wavelength was increased up to 900 nm. The n–π^* transition carbonyl group C=O and π–π^* phenyl group were responsible for the decrease in absorbance with wave length [18]. It can also be caused by the development of color centers at wavelengths of 250 nm [19]. Photo-chemical reactions begin in the Makrofol matrix at that wavelength due to UV absorption, which causes macromolecules to form singlet or triplet ones [18]. The act of plasma destroys the C-H bond for wave lengths larger than 250 nm.

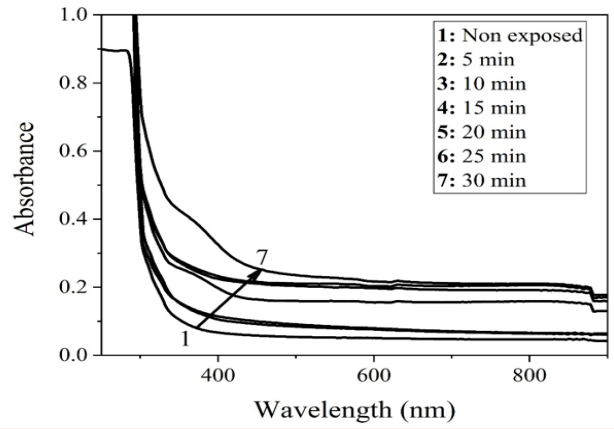

Figure 2: Absorbance pattern of exposed and non-exposed Makrofol films in UV–V_{is}.

Furthermore, increasing the plasma exposure duration to 1800 seconds enhanced the absorbance of the Makrofol films. It is due to the development of conjugated bonds. As a result, a smaller optical band-gap is expected as exposure time is increased [20]. The following formula relates the extinction coefficient k to the refractive index:

$$n^* = n + ik \quad (1)$$

The refractive index's real and imaginary components are indicated by n and k, respectively. The value of k is calculated using the following formula:

$$k = \frac{\lambda\alpha}{4\pi} \quad (2)$$

where λ is the incident light's wave-length. The absorption coefficient α may be computed using the following equation:

$$\alpha = 2.303 \times \frac{Absorbance}{Sample's\ thickness} \quad (3)$$

The coefficient of absorption, α, denotes the amount of light absorbed by the substance, and is thus used to depict differences in the band's configuration.

Band-Gap: The band-gap, E_g, values were obtained using a direct transition method, which is called Tauc's equation that present the information about the band-gap structure transitions [21]

$$\alpha h\nu = B\left(h\nu - E_g\right)^n \quad (4)$$

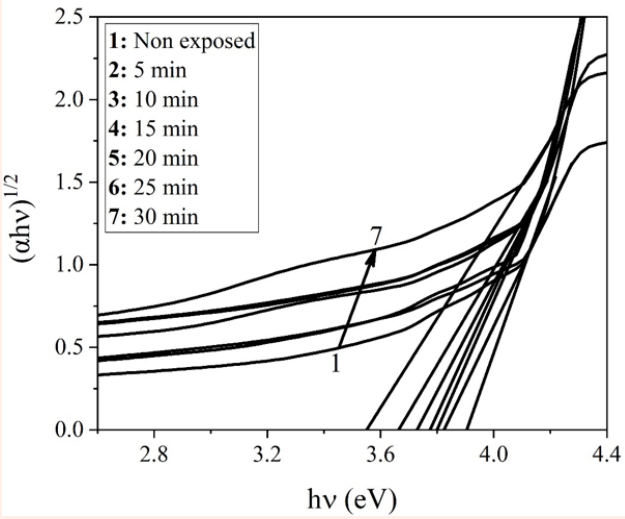

Figure 3: A plot of $(\alpha h\nu)^{1/2}$ against hν.

Where hν signifies the energy of the incoming photon, B denotes a constant, and the index n denotes the nature of the electronic transition. Direct transitions have n values of 1/2 or 3/2, but for indirect transitions it equals 2 or 3 depending on if they are allowed or disallowed, respectively [22]. Plotting the correlation between $(\alpha hn)^{1/n}$ and hn, then extrapolating the linear portion of the curve to cross the hn axis, is used to get optical bandgap as shown in Figures 3-5. Band-gap tends to decrease upon the increase of plasma exposure time to a maximum of 1800 sec. Crosslinking is responsible for the narrowing of the optical band gap. As a result of the produced defects, the amorphous state of the Makrofol films is improved, and localised states are introduced in the band-gap zone, resulting in lower-energy electronic transitions. That is, the creation of chain scissions, conjugated bonds, and unsaturated bonds is caused by the generation of free radicals as a result of plasma radiation on Makrofol. Raising the plasma exposure period increases the rate of free radical generation and the formation of conjugated and unsaturated bonds, resulting in a decrease in the band-gap [20].

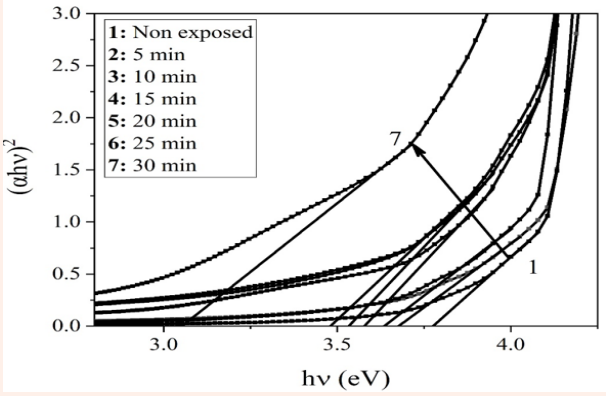

Figure 4: Plot of $(\alpha h\nu)^2$ against hν.

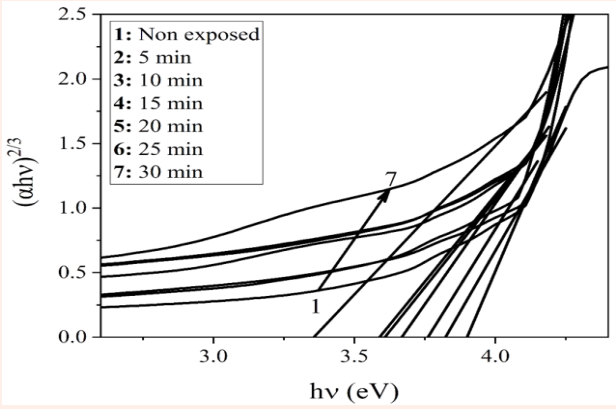

Figure 5: A plot of $(\alpha h\nu)^{2/3}$ versus hν.

The optical band-gap and electronic transition type were calculated using the optical dielectric loss shown in Figure 6 and Tauc's model shown in Figure 3-5.

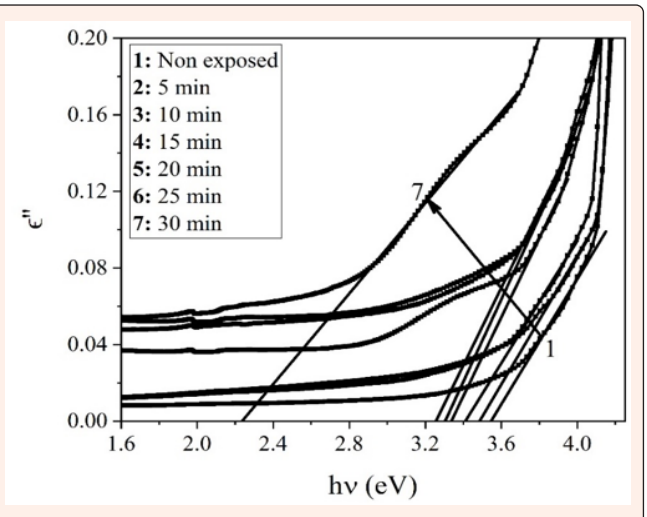

Figure 6: A plot of optical dielectric loss versus hν.

This is because the optical dielectric function is highly dependent on the band structure of the substance. Furthermore, using UV spectroscopy to analyze the optical dielectric function is quite valuable in establishing the band structure of the entire material [22]. the imaginary component of the optical dielectric function ε″ [23,24] is used to explore the electrical transition between unoccupied and occupied states. The optical dielectric loss ε″ can be calculated using the formula below.

$$\varepsilon'' = 2nk \quad (5)$$

The extinction coefficient is k, and the refractive index is n. Figure 6 shows the optical dielectric loss spectra for exposed and non-exposed Makrofol. As shown in Table 1, the optical band-gaps of the films estimated using optical dielectric loss are quite close to those expected using Tauc's model. As a result, the electronic transition type is the only authorized direct transition [24].

Table 1: The optical band gap (from Tauc's model and ε″ vs. hυ) for the non-irradiated and irradiated Makrofol samples.

Exposure Time (sec)	Optical Band Gap from ε″ vs. hυ	Optical Band Gap from Tauc's Model (eV)		
		E_g^2	$E_g^{1/2}$	$E_g^{2/3}$
0	3.55	3.78	3.90	3.90
300	3.49	3.68	3.82	3.82
600	3.41	3.64	3.80	3.76
900	3.34	3.59	3.77	3.67
1200	3.3	3.53	3.73	3.61
1500	3.26	3.48	3.66	3.59
1800	2.24	3.05	3.55	3.36

Materials structure and refractive index: The formula that is used for calculating the refractive index, n, for Makrofol films is [25].

$$\left(\frac{n^2-1}{n^2+1}\right) = 1 - \sqrt{\frac{E_g}{20}} \quad (6)$$

Figure 7 demonstrates how the refractive index varies as the time interval of 1. The index of refraction is increasing on growing the exposure time up to 1800 sec. This pattern matches that of E_g which indicates the authorization of crosslinks. Chain scissions produce active free radicals which allow for the formation of covalent bonds via crosslinking. This explanation is in good agreement with what was previously discovered [26]. The dielectric properties primarily give information on the solid-state optical properties [27]. The dielectric constant varies with photon energy, indicating that strong photon-electron interactions developed in the sample at this energy level.

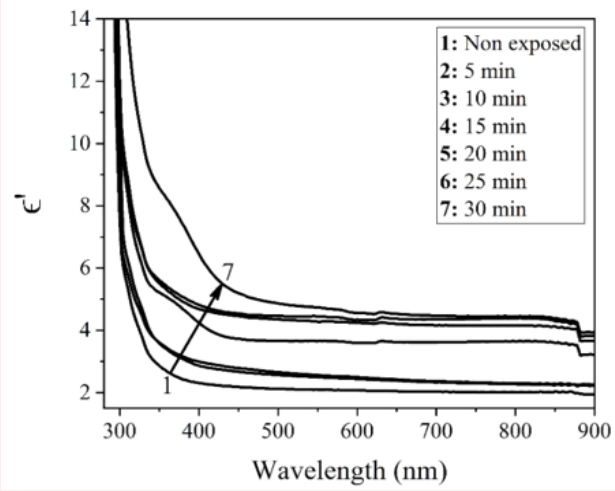

Figure 7: A plot of refractive index changes vs. plasma exposure time.

According to the following formula, the dielectric constant is correlated to n and k [28].

$$\varepsilon' = n^2 - k^2 \quad (7)$$

The values of ε′′ were evaluated and displayed in Figure 8 vs. wave-length. As the exposure time is prolonged to 1800 seconds, the dielectric constant rises. This implies that plasma exposure increases the density of states inside the Makrofol films' forbidden gap [29].

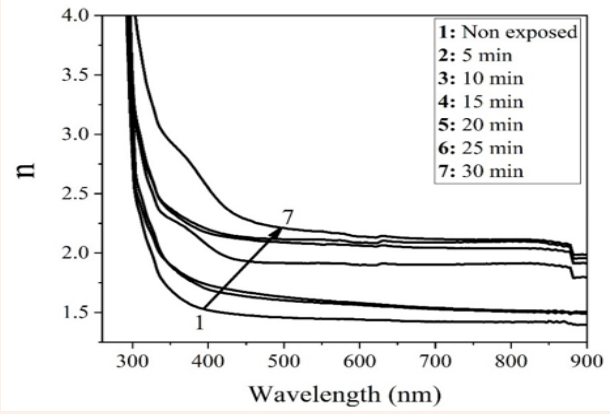

Figure 8: A plot of optical dielectric constant vs. hv.

Conclusion

Plasma irradiation of Makrofol films causes crosslinking dominance, which alters the structural and optical properties of the films under investigation. Due to a plasma exposure length of up to 1800 seconds, the amorphous regions grew larger, and the Makrofol gained flexibility. As a result, our polymer could be a good fit for applications requiring bendability without breaking. The optical band-gap value dropped significantly as the plasma exposure time was increased to 1800 seconds, although the refractive index and optical dielectric constant values rose. Such changes in optical features may lead to improvements in Makrofol films' optical qualities, making them suitable for use in switches, filters, optical coatings, and other applications.

References

1. El Ghazaly M, Aydarous A (2017) Photoluminescence emission spectra of Makrofol® DE 1-1 upon irradiation with ultraviolet radiation. Results in Physics 7: 333-337.
2. Sidorov M, Ivanov O (2010) Nuclear track detectors: design, methods and applications. Nova Science Publishers, Hauppauge, NY, US.
3. Singh NL, Qureshi A, Singh F, Avasthi DK (2007) Modifications of polycarbonate induced by swift heavy ions. Materials Science and Engineering: A 457(1-2): 195-198.
4. Durrani SA, Bull RK (2013) Solid state nuclear track detection: principles, methods and applications. Elsevier Science, Burlington, US.
5. Alhazime AA, Barakat MM, Bahareth RA, Mahrous EM, Aldawood S, et al. (2022) Gamma induced changes in Makrofol/CdSe nanocomposite films. Chinese Physics B.
6. Al-Amri A, El Ghazaly M, Abdel-Aal MS (2017) On induced-modifications in optical properties of Makrofol® DE 1-1 SSNTD by UVB and UVA. Results in Physics 7: 1361-1366.
7. Bahareth RA, Barakat MM, Alhodaib A, Aldawood S, Nouh SA (2021) Tailoring the optical properties of PC/ZnS nanocomposite by γ radiation. The European Physical Journal Applied Physics 93(5): 50402.
8. Al Naim A, Alnaim N, Ibrahim SS, Metwally SM (2017) Effect of gamma irradiation on the mechanical properties of PVC/ZnO polymer nanocomposite. Journal of Radiation Research and Applied Sciences 10(3): 165-171.
9. Alhazime AA, El-Shamy NT, Benthami K, Barakat MM, Nouh SA (2021) Effect of gamma radiation on the structural, thermal and optical properties of PMMA/$Sn_{0.75}Fe_{0.25}S_2$ nanocomposite. Journal of Polymer Engineering 41(2): 119-126.
10. Mishra R, Tripathy SP, Fink D, Dwivedi KK (2005) Activation energy of thermal decomposition of proton irradiated polymers. Radiation Measurements 40(2-6): 754-757.
11. Tommalieh MJ, Barakat MM, Bahareth RA, Mahrous EM, Aldawood S, et al. (2022) Thermal, optical, and color modification in Makrofol VLG 7-1 nuclear track detector due to gamma irradiation. Journal of Macromolecular Science Part B Mar 61(3): 479-493.
12. Nouh SA, Gaballah N, Abou Elfadl A, Alsharif SA (2019) Modification induced by proton irradiation in bayfol UV1 7-2 nuclear track detector. Radiation Protection Dosimetry 183(4): 450-459.
13. Nouh SA, Radwan YE, Elfiky D, Abutalib MM, Bahareth RA, et al. (2014) Structure, thermal, optical and electrical investigation of the effect of heavy highly energetic ions irradiations in Bayfol DPF 5023 nuclear track detector. Radiation Physics and Chemistry 97: 68-74.
14. Fahim E, Bekhit M, Sobhy A, Ali ZI (2020) Exploring polyvinyl alcohol–nickel sulphate composite film for absorbed dose monitoring. Radiochimica Acta 108(3): 231-238.
15. Abdullahi S, Aydarous A, Salah N (2021) Effects of X-ray irradiation on the structural and optical properties of microcrystalline Alq3 powder and its potential dosimetry application. Radiation Physics and Chemistry 188: 109656.
16. Sudha A, Maity TK, Sharma SL, Gupta AN (2019) Gamma irradiation effect on the optical properties of tellurium dioxide films. Nuclear Instruments and Methods in Physics Research Section B: Beam Interactions with Materials and Atoms 461: 171-174.
17. Said HM, Ali ZI, Ali HE (2006) Physical properties of electron beam irradiated poly (vinyl butyral) composites with carbamate, imidazole, and tetrazolium dye. Journal of Applied Polymer Science 101(6): 4358-4365.
18. El-Mesady IA, Rammah YS, Abdalla AM, Ghanim EH (2020) Gamma irradiation effect towards photoluminescence and optical properties of Makrofol DE 6-2. Radiation Physics and Chemistry 168: 108578.
19. Rammah YS, Ibrahim SE, Awad EM (2019) Electrical and optical properties of Makrofol DE 1-1 polymeric films induced by gamma irradiation. Bulletin of the National Research Centre.
20. Gupta SK, Singh P, Kumar R, Kumar S (2015) Gamma radiation induced modifications on physicochemical properties of Makrofol (KG and N) polycarbonate. Advances in Polymer Technology 34(4).
21. Tauc J (1974) Optical properties of amorphous semiconductors. In: Amorphous and liquid semiconductors. Springer, Boston, US, pp. 159-220.
22. Aziz SB, Abdullah OG, Hussein AM, Ahmed HM (2017) From insulating PMMA polymer to conjugated double bond behavior: Green chemistry as a novel approach to fabricate small band gap polymers. Polymers 9(11): 626.
23. Aziz SB, Abdullah OG, Hussein AM, Abdulwahid RT, Rasheed MA, et al. (2017) Optical properties of pure and doped PVA: PEO based solid polymer blend electrolytes: two methods for band gap study. Journal of Materials Science: Materials in Electronics 28(10): 7473-7479.
24. Aziz SB, Abdullah OG, Rasheed MA (2017) A novel polymer composite with a small optical band gap: New approaches for photonics and optoelectronics. Journal of Applied Polymer Science 134(21).
25. Elkhoshkhany N, Abbas R, El-Mallawany R, Fraih AJ (2014) Optical properties of quaternary TeO2–ZnO–Nb2O5–Gd2O3 glasses. Ceramics International 40(9): 14477-14481.
26. Shams-Eldin MA, Wochnowski C, Koerdt M, Metev S, Hamza AA, et al. (2005) Characterization of the optical-functional properties of a waveguide written by an UV-laser into a planar polymer chip. Optical Materials 27(6): 1138-1148.
27. Soylu M, Al-Ghamdi AA, Yakuphanoglu F (2015) Transparent CdO/n-GaN (0001) heterojunction for optoelectronic applications. Journal of Physics and Chemistry of Solids 85: 26-33.
28. Bhavsar VB, Jha D (2016) Study of refractive index dispersion and optical conductivity of PPy doped PVC films. Indian Journal of Pure & Applied Physics (IJPAP) 54(2): 105-110.
29. Brza MA, Aziz SB, Anuar H, Al Hazza MH (2019) From green remediation to polymer hybrid fabrication with improved optical band gaps. International Journal of Molecular Sciences 20(16): 3910.